Friction Experiments on Lunar Analogue Gouges and Implications for the Mechanism of the Apollo 17 Long Runout Landslide.

G. Magnarini[1,2], S. Aretusini[3], T. M. Mitchell[2], G. Pennacchioni[4], G. Di Toro[3,4], H. H. Schmitt[5]

[1] Department of Earth Sciences, Natural History Museum, London, UK.

[2] Department of Earth Sciences, University College London, London, UK.

[3] Istituto Nazionale di Geofisica e Vulcanologia, Rome, Italy.

[4] Dipartimento di Geoscienze, Università degli Studi di Padova, Padua, Italy.

[5] Department of Engineering Physics, University of Wisconsin Madison, Madison, WI, USA.

Corresponding author: Giulia Magnarini giulia.magnarini@nhm.ac.uk

Key Points:

- Rotary friction experiments show that lunar analogue anorthositic-bearing gouges are characterised by high dynamic shear strength

- Friction weakening mechanisms did not contribute to the Light Mantle initiation and other mechanisms are responsible for its hypermobility

- Clast-cortex aggregates may have formed during the Light Mantle emplacement and may be found in the Apollo 17 core samples 73001/73002

Abstract

The Light Mantle landslide is a hypermobile landslide on the Moon. Apollo 17 astronauts collected a core sample of the top 60 cm of the Light Mantle deposit, which is currently being analysed as part of the NASA's Apollo Next Generation Sample Analysis (ANGSA) programme. The origin of its hypermobility remains undetermined, as the proposed mechanisms are difficult to prove because of lack of theoretical and experimental support and the scarcity of field data related to the internal structures of its deposit. Regardless of the emplacement mechanisms, it has been proposed that localised dynamic frictional weakening is responsible for the early stage instability that leads to catastrophic failure. Here, we conduct friction experiments under vacuum to investigate the viability of dynamic friction weakening in lunar analogue anorthosite-bearing gouges (i.e., rock powders). Our results show that localised dynamic friction weakening does not occur in these gouges at loading conditions where, instead, weakening is observed in other materials on Earth. Therefore, possibly other fluidization-related mechanisms contributed to the initiation of the hypermobile Light Mantle landslide. Finally, we describe the microstructures formed in the experiments, including the presence of clast cortex aggregates.

Preliminary investigation of the Light Mantle core samples (73001/73002) shows the presence of similar microstructures. Therefore, our microstructural observations will help the analysis and interpretation of the Apollo 17 core samples, as keys to insights about internal processes occurring during the emplacement of the landslide.

Plain Language Summary

The Apollo 17 mission explored a region on the Moon where a landslide characterised by extraordinary 5-km-long runout is present. Different weakening/lubricating mechanisms have been proposed to explain how the landslide slid for several kilometres away from the headscarp, however no consensus is reached. Therefore, we performed friction experiments reproducing lunar environmental conditions (low gravity and high-vacuum) on anorthosite-bearing powders which simulate the composition of the mountain slope where the landslide occurred. However, the experimental observations rule out the activation of friction-related weakening for the lunar landslide implying that other mechanisms should be considered.

1 Introduction

Friction weakening mechanisms are important in facilitating the runout of large terrestrial landslides (e.g., Erismann, 1979; Goren et al., 2010; Goren & Aharonov, 2007; Hu et al., 2018; Ibañez & Hatzor, 2018; Lucas et al., 2014; Mitchell et al., 2015; Vardoulakis, 2000, 2002; Viesca & Rice, 2012; Voight & Faust, 1982; Weidinger & Korup, 2009)as well as proposed to operate also in extraterrestrial cases, such as on Mars, Ceres, and Iapetus (e.g., Lucas et al., 2014; Schmidt et al., 2017; Singer et al., 2012; Watkins et al., 2015). Similarly to what is described in the mechanics of faulting (e.g., Rice, 2006), it is thought that the localization of the shear stress to a narrow slip zone leads to the onset of frictional weakening mechanisms (e.g., Viesca & Rice, 2012), which are responsible for strength loss and development of high slip velocities already during the early stages of the slope failure (e.g., Alonso & Pinyol, 2010; Pinyol & Alonso, 2010; Voight & Faust, 1982).

The similarity of mechanisms operating in terrestrial long runout landslides and high-slip-rate seismic faulting has been suggested in the light of the role of frictional heating in triggering a series of physical and chemical reactions responsible for friction weakening mechanisms (e.g., Goren & Aharonov, 2007; Vardoulakis, 2002; Voight & Faust, 1982). Examples of frictional heating-triggered weakening mechanisms that have been suggested to explain the hypermobility of some long runout landslides are gas overpressurization (e.g., the Heart Mountain landslide: Goren et al., 2010; Mitchell et al., 2015 and the Vajont landslide: (Ibañez & Hatzor, 2018; Pinyol & Alonso, 2010; Veveakis et al., 2007)), melt production (e.g., the Köfels landslide: Erismann et al., 1977); the Arequipa volcanic landslide (Hughes et al., 2020; Legros et al., 2000) and flash heating (on Iapetus: Singer et al., 2012; on Charon: Beddingfield et al., 2020).

Motivated by the experimental work conducted in the field of fault mechanics, experimental work has been used to investigate friction-weakening mechanisms in terrestrial long runout landslides (e.g., Ferri et al., 2011; Hu et al., 2018; Mitchell et al., 2015; Wang et al., 2017). However, none of these experiments have been conducted on non-terrestrial analogue materials to investigate the long runout mechanisms in extraterrestrial environments.

Evidence for the presence of long runout landslides on the Moon opened important implications for mechanisms of reduction of friction on planetary bodies in the absence of an atmosphere and water availability. The exceptional 5-km-long runout made the Light Mantle landslide deposit one of the primary geological targets of the Apollo 17 mission (Figure 1). Either triggered by impact (Howard, 1973; Lucchitta, 1977) or by seismic shaking (Schmitt et al., 2017), the origin of the hypermobility of the Light Mantle landslide remains unresolved. Howard (1973) suggests that dry fluidization involving regolith particle interactions is the most likely process during the emplacement of the Light Mantle landslide. Instead, Schmitt et al. (2017) speculate that gas fluidization is the principal mechanism, through the release of regolith-implanted solar wind volatiles by agitation of the granular material during the flow. Finally, Kokelaar et al. (2017) propose that the incorporation of erodible regolith during the flow is likely to be implicated in enhancing the Light Mantle mobility. Moreover, also acoustic fluidization remains a theoretically viable mechanism (Melosh, 1979).

Given the importance of friction weakening mechanisms in the development of terrestrial long runout landslides, in this study, for the first time, we perform low atmosphere (high-vacuum) friction experiments on lunar analogue anorthosite-bearing gouges (i.e., rock powders) to test the theoretical viability of thermally-activated dynamic weakening mechanisms in lunar analogue material. We use a high velocity rotary shear apparatus (SHIVA, Slow to High-Velocity Rotary Shear Apparatus, Di Toro et al., 2010), at the Istituto Nazionale di Geofisica e Vulcanologia in Rome (Italy) to determine the viability of thermally-activated dynamic weakening mechanisms that could explain the exceptional runout of the Light Mantle landslide. We present the results of the SHIVA friction experiments, X-Ray Powder Diffraction (XRPD) analysis and high-resolution (Field Emission Gun Scanning Electron Microscope (FEG-SEM) microstructural observations. Finally, we comment on the implications for the emplacement mechanism of the Light Mantle landslide.

1.1 The Light Mantle Landslide

The Light Mantle landslide originated from the summit of the NE-facing slope of the South Massif about 70-110 Ma (e.g., Lucchitta, 1977; Schmitt et al., 2017) and its deposit extends for about 5 km on the valley floor of Taurus-Littrow Valley, the landing site of the Apollo 17 mission in 1972 (Figure 1). The total plan-view travel length (L) of the Light Mantle, from the top of the source region to the terminal, is about 10 km. Given the height (H) of the South Massif is 2.2 km, the Light Mantle is charactrised by an H/L ratio of 0.22, which therefore identifies the Light Mantle as hypermobile (e.g., Hsü, 1975; Iverson, 1997; Legros, 2002).

The lack of a clear headscarp casts doubts on the origin and nature of the Light Mantle deposit. Whether it constitutes only the destabilization of regolith or also the failure of rocky substrate, the highly mobile mass generated morphological features that Lucchitta (1977) describes as similar to other secondary textures attributed to the high energy-impact of the ejecta from Tycho crater; more generally, Magnarini et al. (2021) attribute the longitudinal morphological structures of the Light Mantle deposit to the high-speed nature of the mass emplacement. Therefore, the emplacement of the Light Mantle was characterised by high velocity. However, the origin of such high velocity remains undetermined, as it does for other long runout landslides in the Solar System (Lucas et al., 2014).

Although an obvious headscarp is not visible (Figure 2a), the upper part of the NE-facing slope of the South Massif shows evidence of rocky outcrops, supposedly exposed after the slope

failure, from where numerous boulder falls have been identified (Bickel et al., 2021; Hurwitz & Kring, 2016; Schmitt & Cernan, 1973). Such region at the summit of the South Massif is characterized by low reflectance material, smoother than the surrounding terrains, that Hahn et al. (2019) interpret as impact melt from the Tycho impact event. The observation of impact melt and blocky material at the summit of the South Massif may well suggest that the impact of Tycho ejecta triggered the landslide that generated the Light Mantle deposit, mobilizing not just surficial regolith but also rocky material.
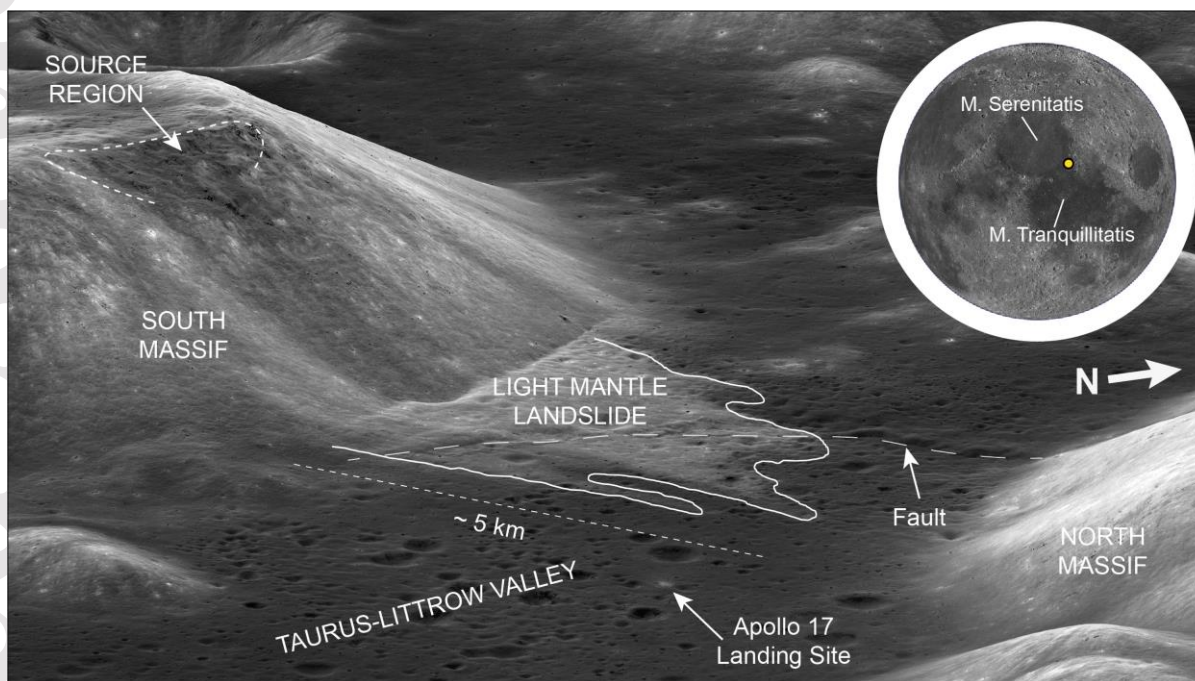

Figure 1 – Oblique view of Taurus-Littrow Valley on the Moon. The Light Mantle appears as a high albedo deposit superposed on the dark basaltic material that fills the valley. The South Massif is part of a relief system that forms the crater rims of Mare Serenitatis and Mare Tranquillitatis, and it is mainly constituted of anorthositic breccia. Image: LROC NAC M1266925685.

Samples collected from the boulders and regolith at the base of the South Massif, and the landslide deposit during the Apollo 17 mission (Figure 2c) have been used to infer the composition of the South Massif. The sample analysis shows that the South Massif bulk composition is that of an anorthositic breccia, with contribution from other lithologies such as noritic breccia and dunite (e.g., Ryder et al., 1992; Wolfe et al., 1981). A core sample of the top 60 cm of the Light Mantle deposit (A17-73002/73001) was collected during the Apollo 17 mission at station 3 and left unopened until the end of 2021. As part of the NASA Apollo Next Generation Sample Analysis (ANGSA) program (Shearer et al., 2020), current mineralogical and petrographic analysis of the sample 73002 show that the material contains different lithologies that include highland lithologies from the South Massif, and mare basalts lithologies (e.g., Bell et al., 2022; Shearer et al., 2022; Simon et al., 2022; Sun et al., 2022). However, the highland,

anorthositic-bearing component is the dominant part, compared to mare basalt fragments and other rare, newly sampled pyroclastic litholigies (Simon et al., 2022).
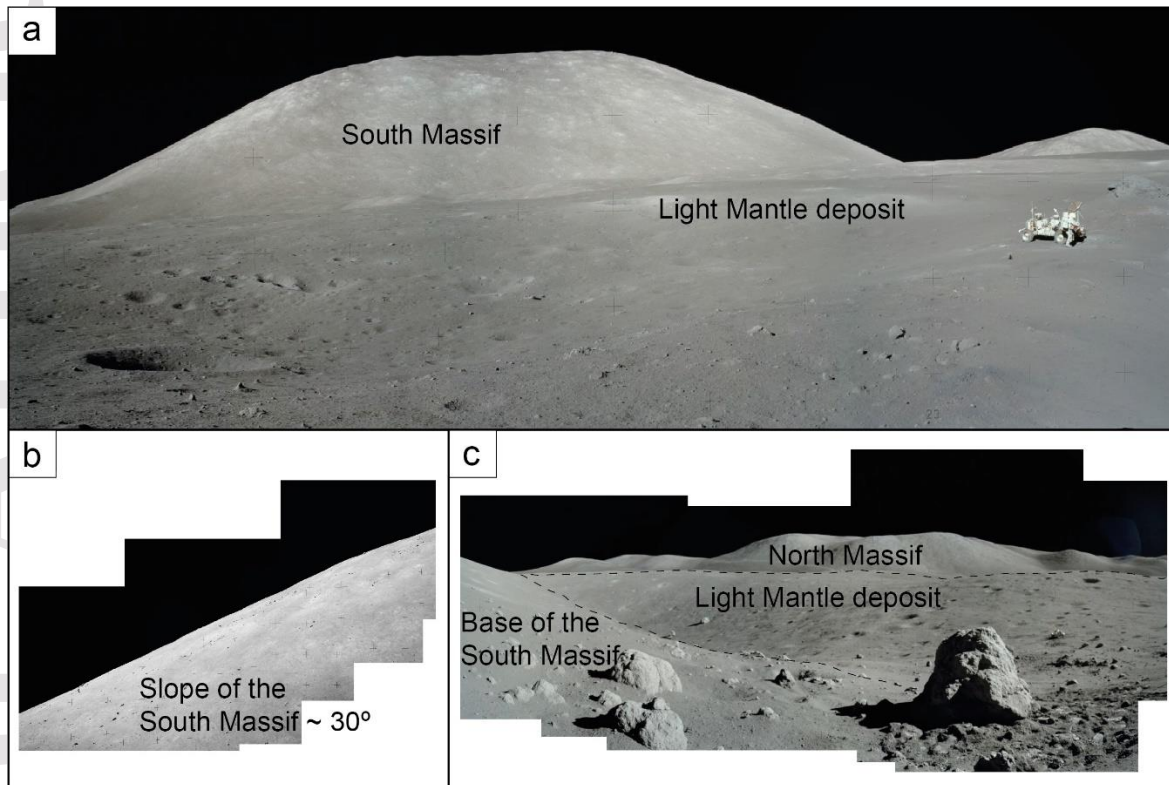

Figure 2 – Apollo 17 lunar ground photos of the South Massif and the Light Mantle landslide deposit. a) View of the South Massif near Shorty Crater, at the distal end of the Light Mantle landslide deposit; photomosaic from mission images AS17-137/21009-21016 b) Close view of the slope of the South Massif; photomosaic from mission images AS17-144/22063-22071. c) Close view of the base of the South Massif and the proximal area of the Light Mantle deposit; the larger boulder on the righ-hand side of the image is about 1.5 m height; photomosaic from mission images AS17-137/20944/20945/20947/20949/20954/20955/20956.

2 Methods

We conduct friction experiments under vacuum to investigate the viability of dynamic friction weakening in lunar analogue anorthosite-bearing gouges (i.e., rock powders). The sets of experiments are meant to investigate such mechanisms and their implications for the emplacement of the Light Mantle deposit, although the full in-vacuum, *in-situ* nature and origin of the Light Mantle debris cannot be duplicated under terrestrial conditions.

We used Proterozoic anorthosites of the Scandinavian Shield, provided by the European Space Agency Sample Analogue Curation Facility (ESA SAFC). These Proterozoic anorthosites are used as analogue of the composition of the South Massif. We prepared the experimental gouges by crushing and sieving (< 250 µm) the anorthosite-bearing rock. The experimental parameters

were chosen so to simulate the sliding conditions of material along an inclined surface similar to the slope of the South Massif.

To conduct the friction experiments we used SHIVA (Slow to High Velocity Apparatus, Di Toro et al., 2010; details on design and capability are provided in Di Toro et al. (2010) and Niemeijer et al. (2011)), a rotary shear machine capable of simulating the fast acceleration, slip rate and large displacement occurring during landslide collapse (Mitchell et al., 2015) or earthquake slip (Aretusini et al., 2021; Cornelio et al., 2019; Fondriest et al., 2013; Niemeijer et al., 2012; Passelègue et al., 2016; Smith et al., 2015; Violay et al., 2014). During the main phase of each experiment, the sample is sheared at a costant velocity of 1 m s^{-1}. Other materials tested at this velocity display intense weakening (see Figure 4 and references within), and out objective is to see whether the Light Mantle deposit analogue material weaken accordingly at high speed. We applied an acceleration of 0.8 m s^{-2} (the minimum acceleration applicable with SHIVA), which corresponds to the acceleration of an object along a surface inclined with an angle of 30º under lunar gravity (~ 1.6 m s^{-2}). This angle corresponds to a slightly higher angle than the current NE-facing 28º slope of the South Massif (Figure 2b). SHIVA is equipped with a vacuum pump (Pfeiffer Hi-Cube) to create a minimum pressure of 10-4 mbar in a chamber surrounding the samples.

The source region of the Light Mantle landslide does not appear with an obvious headscarp and a clear surface of failure. This uncertainty prevents estimating the depth of the detachment surface. Therefore, we chose three different normal stresses to apply so that they would correspond to the load applied by slides of various thicknesses constituted of material with a density of 2500 kg m^{-3} (anorthosite density varies between 2200 kg m^{-3} and 2600 kg m^{-3}), under lunar gravity. We decided not to perform experiments with normal stresses lower than 2MPa, as this would compromise the quality of the detection of the traction evolution with slip due to the low resolution of the torque gauge. We chose the following normal stresses, for which we provide the corresponding thickness under the simulated conditions described above: 2 MPa = 500 m; 5 MPa = 1250 m; 10 MPa = 2500 m. As we mentioned, there is no topographic evidence of the depth of the failure surface, therefore the considered thicknesses may correspond to overestimations of the slide that generated the Light Mantle landslide.

Sheared gouge samples were consolidated with epoxy under vacuum. Polished petrographic sections were obtained, from which thin sections of sheared gouges were cut orthogonal to the slip surface and tangential to the slip vector. To analyse the thin sections, we used TESCAN Field Emission Scanning Electron Microscope (FESEM) at the Department of Geoscience, University of Padua (backscattered mode; acceleration voltage 5 kEv; working distance 3.06 mm).

We conducted X-Ray Powder Diffraction (XRPD) analysis of the original anorthosite-bearing gouge and the sheared gouges at the Department of Earth Sciences at University College London (continuous scanning mode; step size 0.017º 2Theta; scan step time 254.5442 s; measurement temperature 25º; generator 30mA, 40 kV).

3   Results

3.1 Friction Experiments and XRD Analysis

A total of six experiments were performed at a constant normal stress of 2 MPa, 5 MPa, 10 MPa, and both at room humidity and in high vacuum ($< 5e^{-4}$ mbar) to simulate the absence of a lunar atmosphere (Table 1). Gouge samples were sheared simulating a landslide runout (up to 5 m displacement) with a single slip pulse at constant slip rate of 1 m s^{-1}, which was reached applying an initial acceleration of 0.8 m s^{-2}.

Table 1 – List of friction experiments conducted on anorthosite-bearing gouges.

Experiment Code	Sample Weight (g)	Acceleration (ms^{-2})	Peak Velocity (ms^{-1})	Slip (m)	Normal Stress (MPa)	Pressure (mbar)
s1668	6	0.8	1	5	2	High Vacuum
s1669	6.15	0.8	1	5	5	High Vacuum
s1670	6.08	0.8	1	2	10	High Vacuum
s1671	6.06	0.8	1	5	5	Room Humidity
s1673	6.06	0.8	1	2	10	Room Humidity
s1674	6.08	0.8	1	5	2	Room Humidity

Figure 3 show the results of the friction experiments. A small reduction of friction coefficient of ~ 0.1 occurs at the highest normal stress experiments, both at room humidity and high vacuum conditions. However, considering the high slip rate applied (1 m s^{-1}) and the tested slip displacement (up to 5 m), overall the friction coefficient remains high (~ 0.6), independently of the applied normal stress (2, 5, and 10 MPa) and environmental conditions (room humidity and high vacuum). Therefore, we conclude that the anorthosite-bearing material has a high dynamic shear strength. We do not observe dynamic weakening at conditions where it is seen for many other gouge compositions (Figure 4).
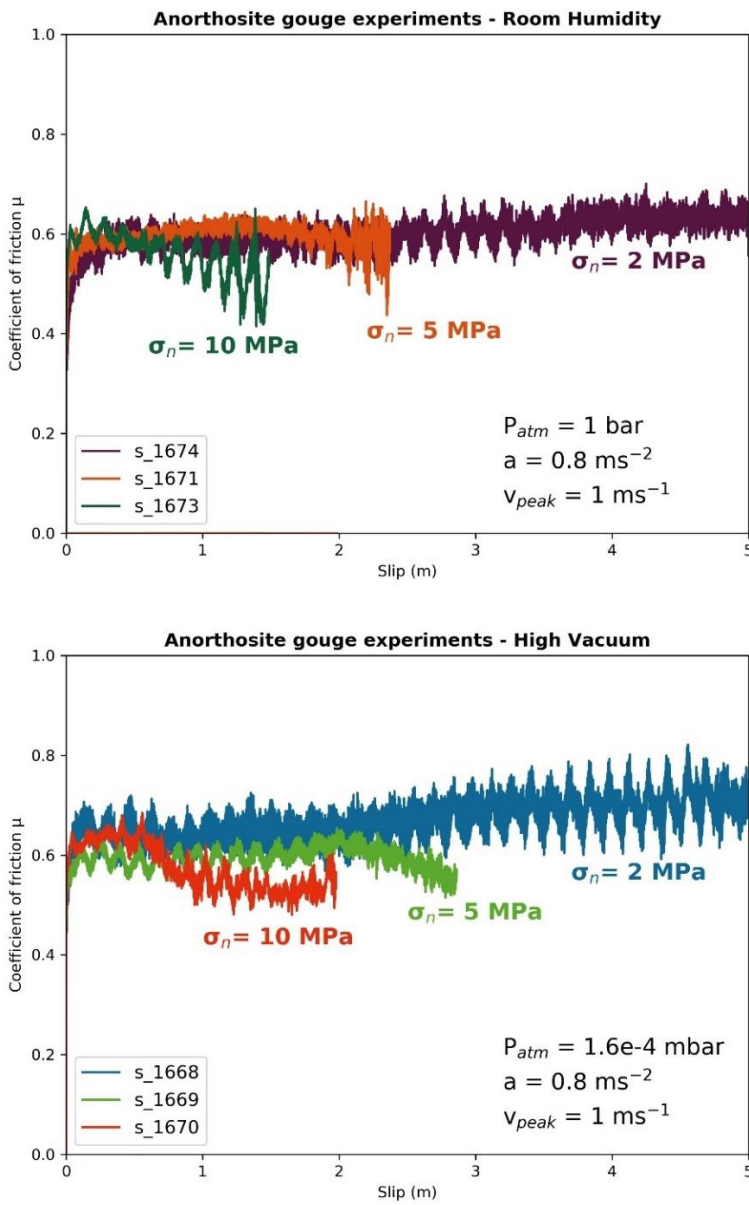
Figure 3 – Results of the friction experiments conducted on anorthosite-bearing gouges.
Upper panel shows the results of the experiments conducted at room humidity. Lower panel shows the results of the experiments conducted in high vacuum ($< 5e^{-4}$ mbar) conditions used to simulate the absence of a lunar atmosphere.
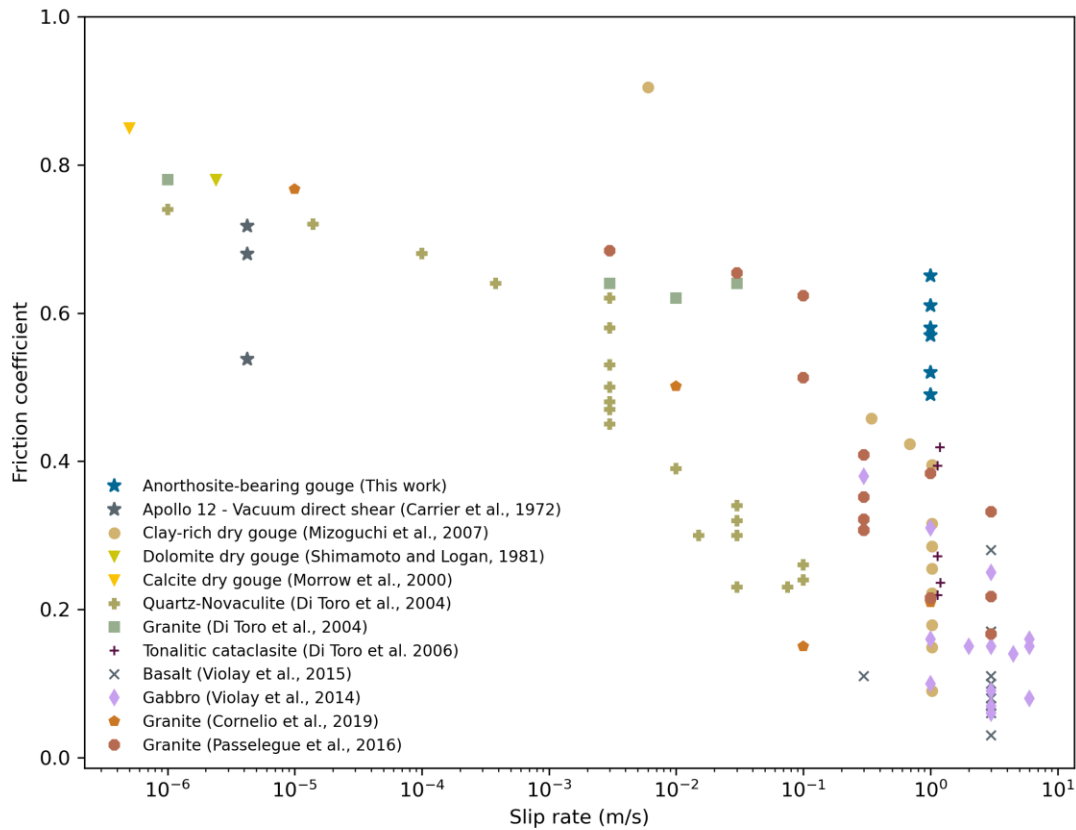
Figure 4 – Values of the coefficient of friction from slow to high slip rates found in laboratory experiments performed on rocks. The plot compares coefficient of friction vs slip rates of literature data and this work results. At the slip rate applied for the experiments in this work (1 m s^{-1}) a sharp decrease in the coefficient of friction is observed in literature data regardless of the lithology and environmental conditions (room humidity, presence of liquid water, etc.). Our results show that anorthositic-bearing material has a high dynamic shear strength, as dynamic weakening is not seen at conditions where it occurs for other rocks. (Note: the reported values of the friction coefficient were measured at slip distances larger than 300 mm and obtained in rotary shear configuration with the exception of friction data from Morrow et al. (2000, triaxial configuration), Shimamoto & Logan (1981, triaxial configuration) and Carrier et al. (1972, direct shear configuration) that were measured for slip distances shorter than 10 mm. Data points of Carrier et al. (1972) are extrapolated from the shear stress and shear values obtained from Carrier et al. (1991), and the experimental velocity from Bromwell . (1966)).

We analysed the original gouge sample and the gouges recovered after the friction experiments. To identify the formation of new mineral phases during the experiments, we compared the X-Ray diffractogram of the gouges sheared at room humidity and at high vacuum to the spectrum of the original gouge (Figure 5). We do not observe the presence of new phases in the sheared gouges.
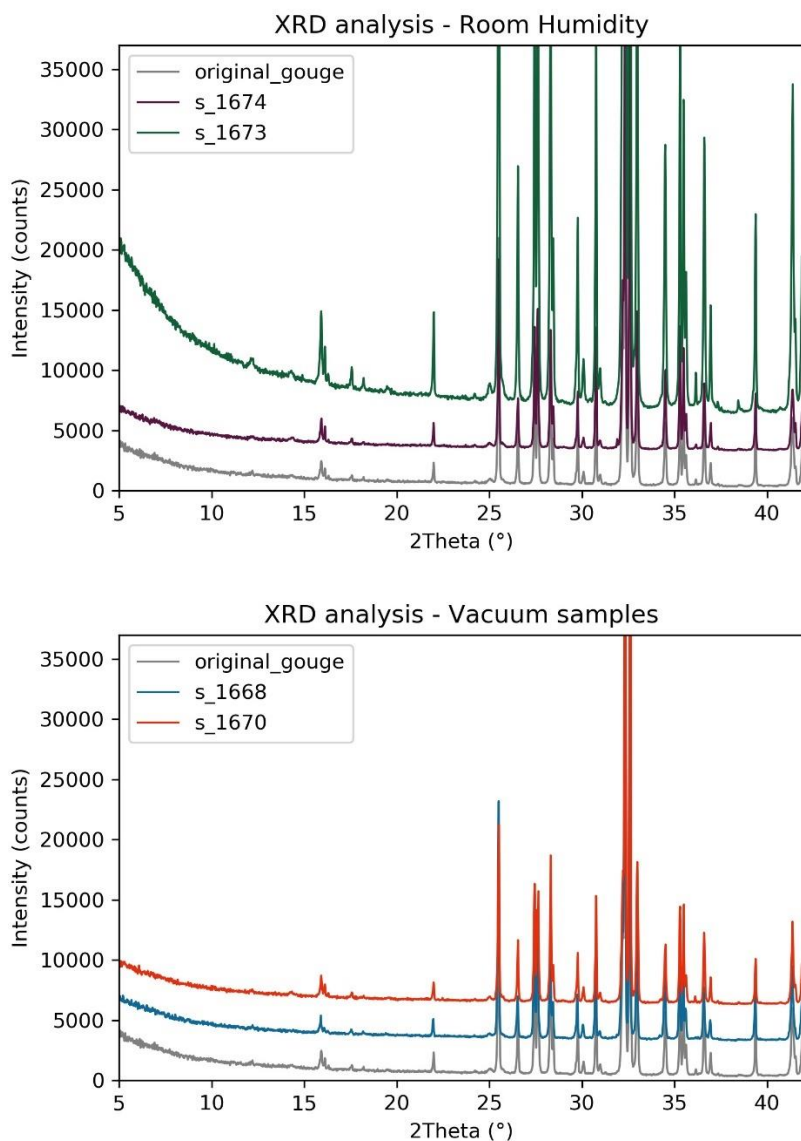
Figure 5 – Results of the XRD analysis conducted on anorthosite-bearing gouges. Upper panel shows the comparison between the diffractogram of the original gouge (grey curve) and the diffractogram of the gouges sheared at room humidity (burgundy curve, 2 MPa; green curve, 10 MPa). Lower panel shows the comparison between the diffractogram of the original gouge (grey curve) and the diffractogram of the gouges sheared in high vacuum conditions (blue curve, 2 MPa; red curve, 10 MPa). The colours in these plots match the colour used to show the results of the friction experiments.

3.2 Microstructural Observations.

We selected FESEM images of the s_1668 experiment sample (2 MPa normal stress; 1 m/s target slip rate; 5 m slip displacement; high vacuum conditions) to investigate the microstructures, as its conditions were the most relevant to the study of the Light Mantle landslide (see discussion).

From the analysis of the sample, we observed strain localization close to the slip zone. Moving away from the slip zone, we identified three distinct microstructural zones (Figure 6, Figure 7):

1. Zone "1", the closest to the slip zone, is characterised by the presence of highly comminuted matrix, clast aggregates with solidified melt, which we named "melt balls", and rounded clast-cortex aggregates (CCAs) (Figure 6c; 8a, d). The "melt balls" are about 10 to 20 µm in size. The particles forming the melt aggregates are less than 1 µm and present zonation, with the border brighter (Ca-enriched) than the nucleus (Na-enriched) (Figure 8c, e). A similar variation in colour appears between the microclasts and the melt, lighter grey and darker grey, respectively (Figure 8e). The CCAs are made of a central clast surrounded by fine-grained fragments derived by the breaking of the clast edges through spallation (Figure 8a, b, d).
2. Zone "2" shows incipient CCAs about 20 µm in size that have a pseudo-rounded shape, at times slightly angular compared to the CCAs observed in zone "1" (Figure 6c). Angular clasts up to 40 µm in size are also present within a coarser matrix compared to the matrix observed in zone "1". These angular clasts show initial stages of spallation (Figure 8b).
3. Zone "3" consists of relatively coarse angular clasts that are closely related to the starting gouge (Figure 6d).
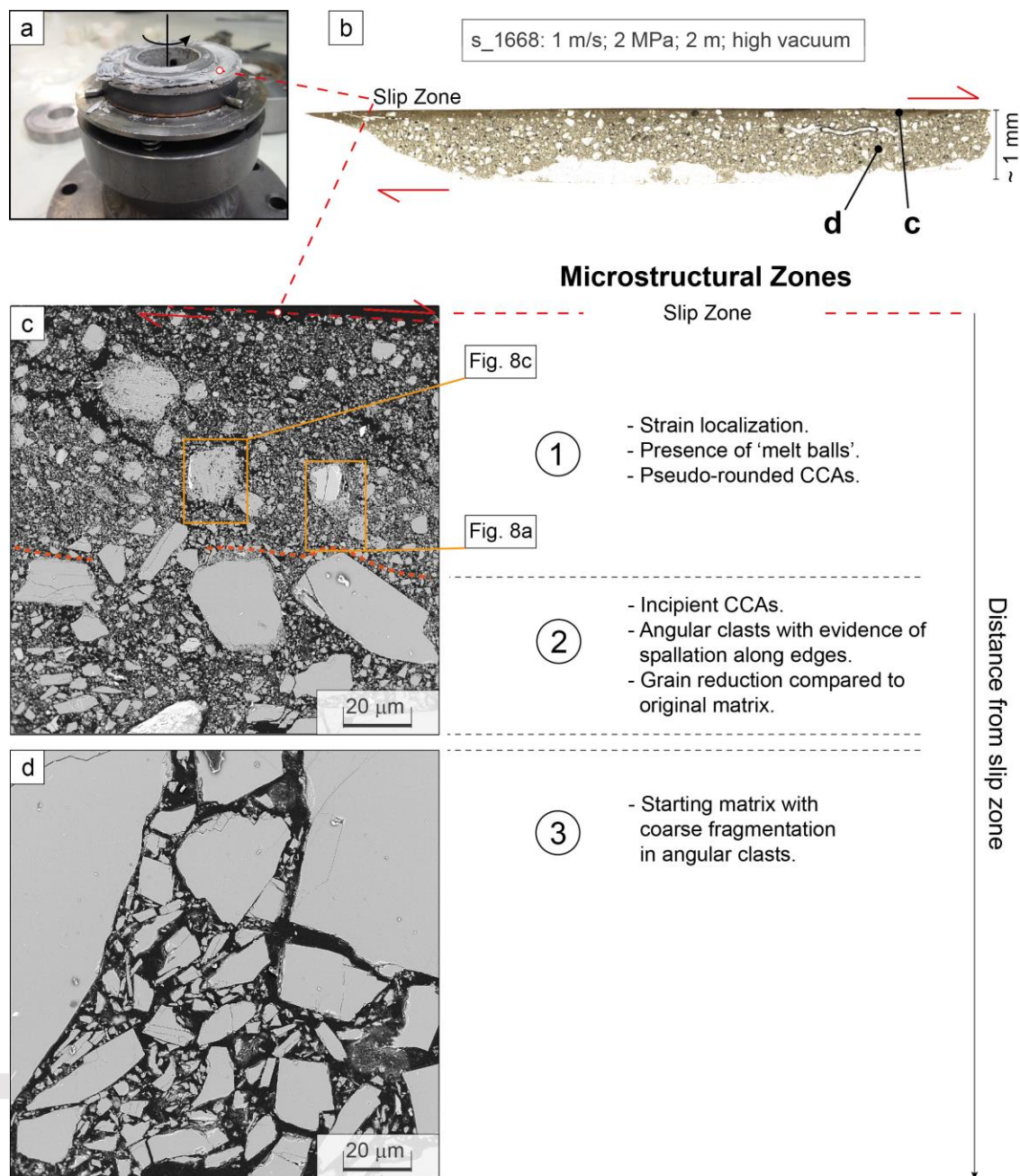
Figure 6 – Microstructural zones identified within the gouge sample of the experiment s_1668. a) Example of a sheared gouge before a sample is collected for thin section analysis; sense of shear (right-lateral) is indicated by the arrow. b) Scan of the petrographic thin section of the gouge sample of experiment s_1668 (1 m/s; 2 MPa; high vacuum); the location of panel c) and d) is annotated on the image of the thin section. c) and d) Examples of the three microstructural zones identified within the gouge sample: with increasing distance from the slip zone (identified with a dashed red line; sense of slip is provided by two red arrows), we identified a zone 1 characterised by strain localization, presence of 'melt balls' and pseudo-rounded Clast Cortex Aggregates (CCAa) (orange boxes in c) show the location of Figure 8a and 8c); the orange dashed line in c) separate zone 1 from zone 2, which is characterized by an overall grain reduction compared to the

original matrix, incipient CCAs, angular clasts with evidence of spallation along edges; zone 3 is characterized by angular clasts that represent coarse fragmentation of the starting matrix.
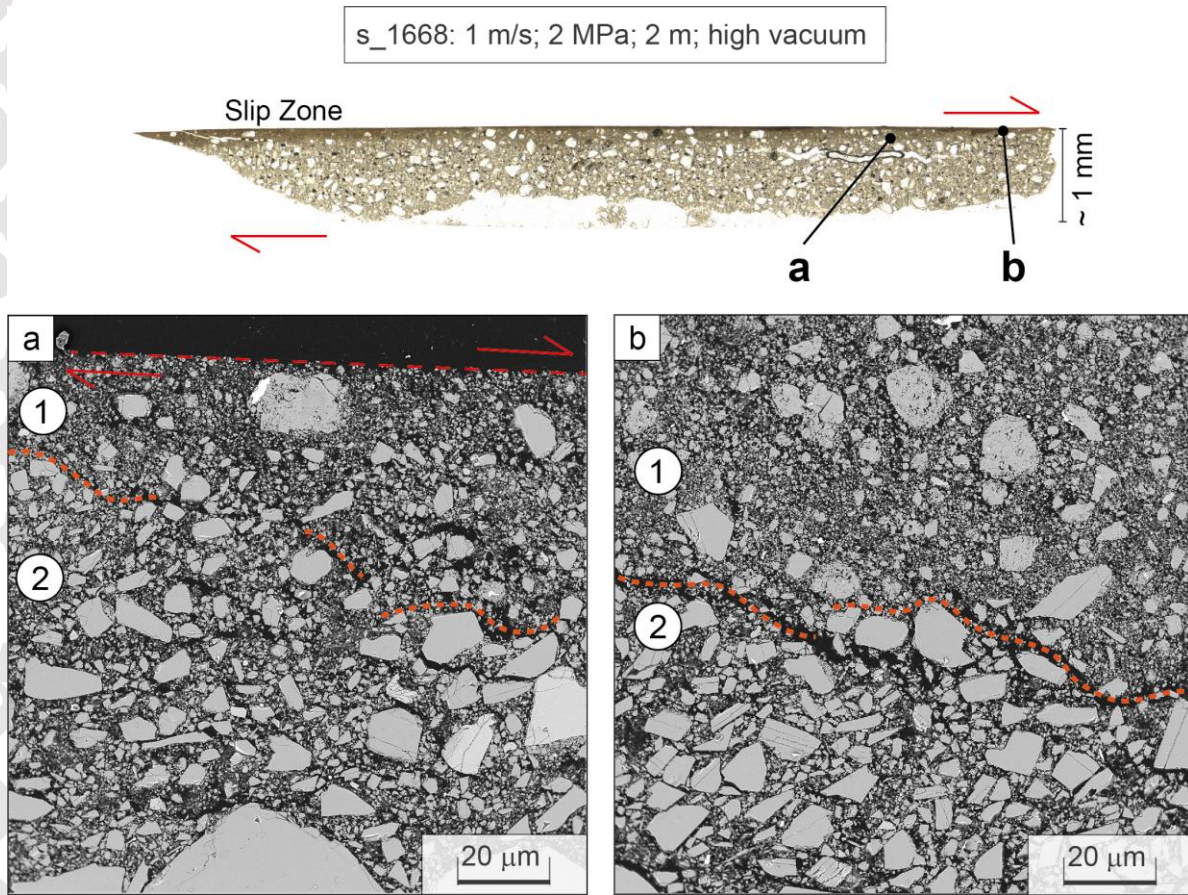

Figure 7 – Examples of transition from microstructural zone 1 to zone 2. The location of panel a) and b) is annotated on the top image of the thin sectionof experiment s_1668. Full description of the characteristics of microstructural zones is provided in the main text and in the caption of Figure 6. The orange dashed line in both panels separate zone 1 from zone 2. In panel a), the red dashed line identifies the slip zone and the two red arrows provide the sense of slip.
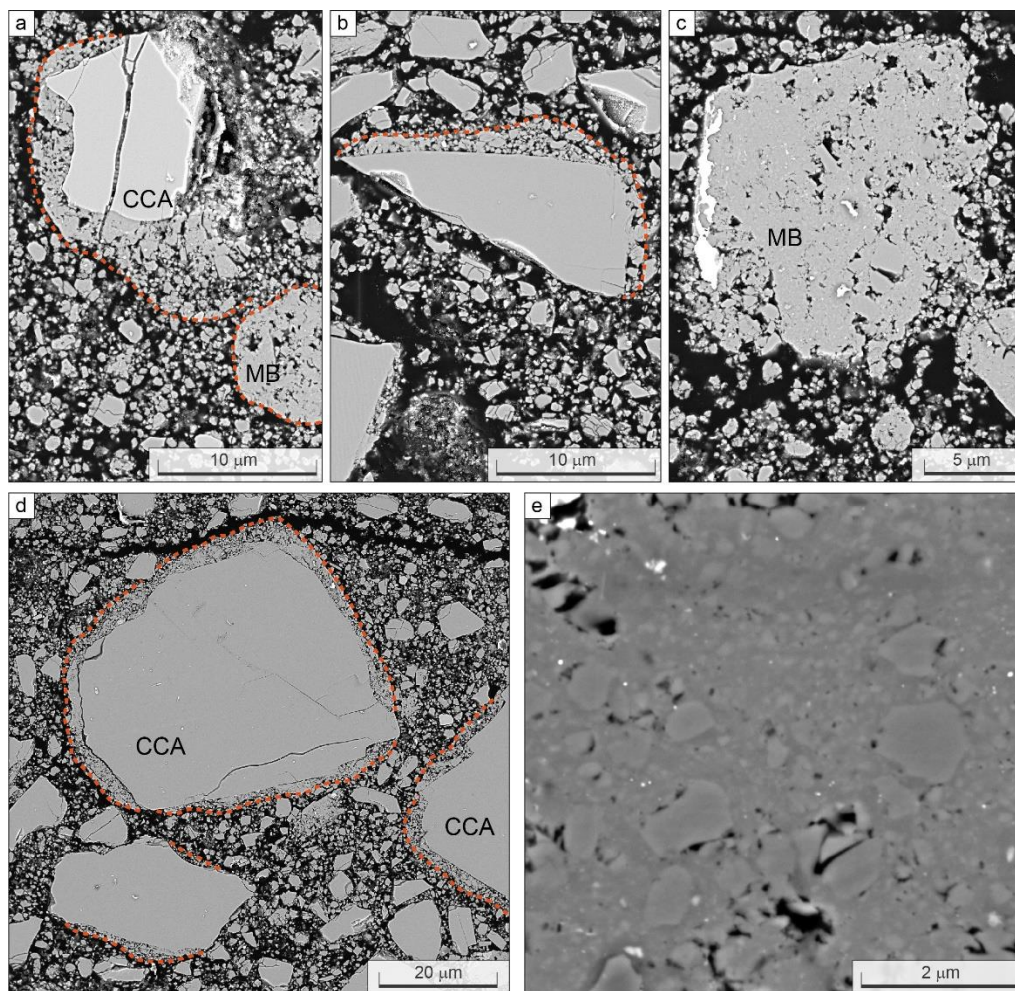
Figure 8 – Details of the microstructures observed within the gouge sample sheared at 1 m/s under vacuum conditions (experiment s_1668). a) Examples of a clast-cortex aggregate (CCA) and a "melt ball" (MB). b) Example of an angular clast showing initial formation of a clast cortex through spallation of the clast edge. c) Example of a melt aggregate (MB). d) Examples of CCAs and of an incipient CCAs (lower left). e) Close-up of the structure of a melt aggregate.

4   Discussion.

The absence of an obvious headscarp suggests that the slope failure that generated the Light Mantle landslide did not affect the fractured bedrock of megaregolith of the South Massif but it only mobilized the upper layers of regolith. However, rocky outcrops are seen in the upper part of the South Massif, which may imply some degree of involvement of bedrock in the failure. In this regard, the Light Mantle landslide differs from more canonical morphologies of other long runout landslides, for which an headscarp and a surface of failure can be easily identified from both orbital and ground imagery. Such uncertainties make it difficult to find meaningful analogues of the Light Mantle deposit, greatly limiting our understanding of the nature and dynamics Light Mantle slide. Therefore, our study does not

comment on the dynamics of the Light Mantle based on morphological comparison with other long runout landslides.

Regardless of the triggering mechanism and of the morphology of the Light Mantle, our study aims to investigate the availability of friction weakening mechanisms in anorthosite-bearing lunar analogue materials in order to further our knowledge of the processes involved in lunar mass-wasting event. Our results show that, regardless of the assumed thickness of a theoretical slide, friction weakening mechanisms in anorthosite-bearing gouges are not supported by experimental evidence. In the next section we comment on our experimental results, on their implications for the mobility of the Light Mantle and on their significance for the analysis of the Apollo 17 core sample 73002/73001.

4.1 Implications for the Mechanism of the Apollo 17 Light Mantle Landslide

This uncertainty about the headscarp and the surface of failure prevents estimating the volume of the mobilised material, as well as the depth of the detachment surface. Despite this, from observation of the current topography of the South Massif, it is certain that the thickness of the failed slope section did not reach 500 m, which is the thickness value extracted from the experiments performed applying the minimum normal stress of 2 MPa. However, given that we do not record dynamic weakening at experimental conditions that overestimate the normal stress, thickness and slope of the landslide, we conclude that dynamic weakening mechanisms did not take place during the initial stages of the mass-wasting event. Although the results from our experimental work do not provide new insights on the actual operating mechanism during the Light Mantle emplacement, they allow us to rule out dynamic friction weakening mechanisms as dominating mechanism. Therefore, that leaves dry fluidization (Howard, 1973), gas fluidization (Schmitt et al., 2017), acoustic fluidization (Melosh, 1979), and regolith entrainment (Kokelaar et al., 2017) available for consideration (Figure 9).

Mobility enhancement due to material entrainment (e.g., Mangeney et al., 2010) is a likely contribution to the emplacement of the Light Mantle deposit (Kokelaar et al., 2017). The lunar surface is subject to constant regolith formation, estimated to be about 1 mm/Myr from ~3.5 Ga to present day (Hörz et al., 1991). As the lunar regolith angle of repose is found to be ~40º (Carrier et al., 1991), the slope of the South Massif is well within the range of stability, therefore a certain thickness of regolith should be expected to accumulate above the fractured bedrock of megaregolith that derives from the anorthositic breccia. The regolith thickness available depends on the time span between material mobilization downslopes.

Mechanisms of dry fluidization have been proposed to explain the hypermobility of some terrestrial avalanches. At a fundamental level, mechanisms of dry fluidization involve the interaction of the clasts within the fast moving debris, which collisions exploit the high kinetic energy available to generate dispersive stresses, thus reducing frictional resistance (e.g., Davies, 1982; Davies & McSaveney, 2009; Heim, 1932; Hsü, 1975). Dynamic fragmentation (Davies & McSaveney, 2009, 2012) sets at the lower part of a slide, near the basal surface, where the stresses are higher. There is no topographic evidence for constraining the thickness of the mobilized material along the slope of the South Massif and, therefore, to assess the normal stress applied at the base of the slide. The mobilized material involved an undetermined volume of lunar regolith, that is material <2 mm in size, which would offer a minimal contribution to the development of mechanical fluidization via dynamic fragmentation. However, evidence of rocky outcrops at the summit of the South Massif suggests that the detachment failure may have also

involved consolidated rock and not only loose regolith. Such rocky component would contribute to providing energy to the system through collisions and fragmentation, according to the dynamic fragmentation theoretical work (e.g., Davies & McSaveney, 2002, 2009).

Gas fluidization proposed by Schmitt et al. (2017) remains a speculation, as the amount of solar wind implanted volatiles is not constrained. In addition to the quantity necessary to fluidize a lunar avalanche, the depth at which such volatiles are implanted and accumulated would determine the fraction of regolith that is fluidized. Therefore, depending on the thickness of the avalanche, a parameter that is unknown, such implanted volatiles may only be able to fluidize the upper portion of the whole mobilised loose and consolidated debris.
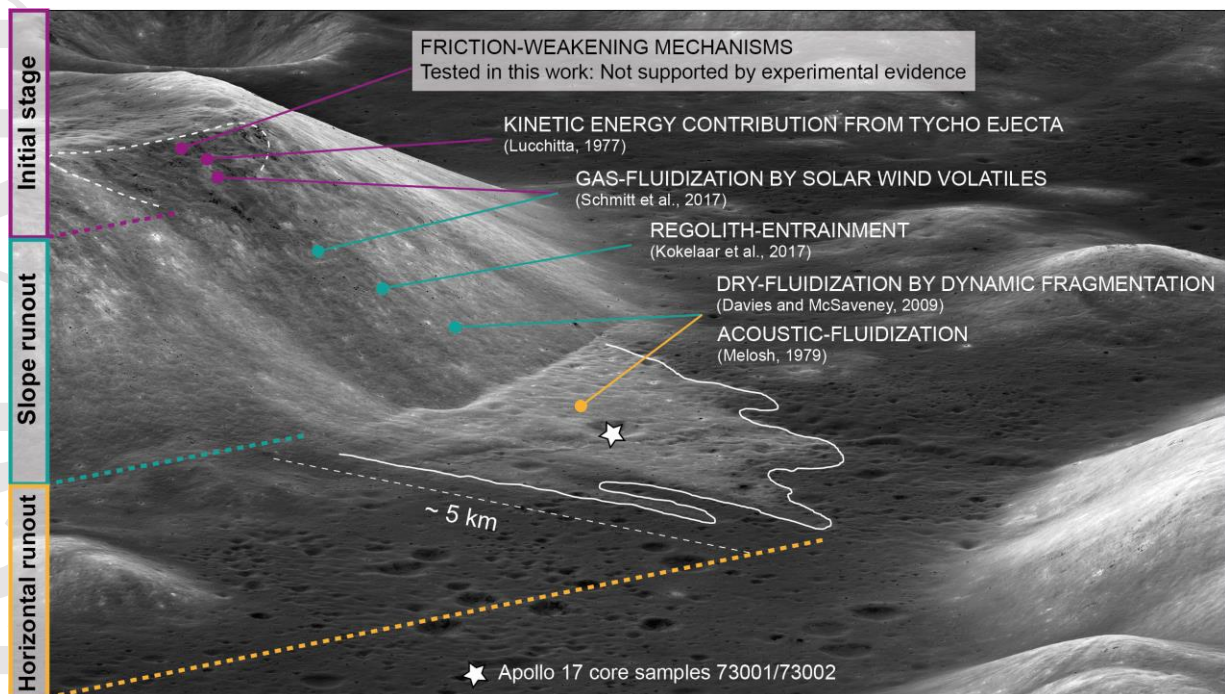

Figure 9 – Map of the possible mechanisms contributing to generating the excessive runout of the Light Mantle landslide. The runout profile is divided into three sections: initial stage, slope runout, and horizontal runout. The figure shows the locations where the proposed mechanisms would be expected to operate. The star symbol shows the location where the core samples 73002/73002 of the Light Mantle deposit were extracted using a drive tube during the Apollo 17 mission in 1972. Image: LROC NAC M1266925685.

The apparent unicity of a low-slope avalanche deposit on the Moon represented by the Light Mantle (Kokelaar et al., 2017) may be due to the difficulty in developing friction-weakening of the anorthositic-bearing material forming the highlands slopes on the Moon. However, in a global study about lunar granular flows, Bickel et al. (2022) found that younger terranes feature higher spatial flow feature densities than older surfaces. Therefore other low-slope and long runout landslides in older anorthositic terranes may have occurred in the past but have been buried, thus, their record have been lost. In fact, Schmitt et al., (2017) suggest the

existence of a second, older landslide deposit, partially buried by the Light Mantle landslide deposit. Alternatively, friction weakening mechanisms are not available in anorthosite-bearing material, suggesting that the occurrence of a long runout deposit such as the Light Mantle could be reliant on other mechanisms, which availability and/or contribution is difficult to assess.

Finally, it cannot be entirely excluded that the mobility of the Light Mantle was, instead, facilitated by the high-energy impact of projectiles ejected by the Tycho impact event (Hahn et al., 2019; Lucchitta, 1977) and, thus, the necessity of friction weakening mechanisms may be excluded (Lucchitta, 1977).

4.2 Clast Structures

Clast-cortex aggregates (CCAs) have been described in the basal slip zone of large landslides (e.g., Anders et al., 2010; Beutner & Gerbi, 2005), as well as in slipping zones of tectonic faults (Boutareaud et al., 2010; e.g., Rempe et al., 2014; Smith et al., 2011). Rempe et al. (2014) studied CCAs in calcite-bearing gouges and their results indicate that CCAs form at low normal stresses (< 5 MPa); in room-dry or vacuum conditions; and they better develop with increasing displacement (up to 5 m). Although anorthosite-bearing material appears to have a high dynamic shear strength, our results show that CCAs are developed at similar low-strain and dry conditions. This may suggest that CCAs may have formed during the Light Mantle landslide emplacement and that they may have been possibly preserved within the final deposit, as shown for the larger Heart Mountain landslide by Beutner and Gerbi (2005) and Anders et al. (2010).

A core sample of the top ~60 cm of the Light Mantle deposit was collected in a central location of the deposit during the Apollo 17 mission using a double drive tube (Samples 73002 and 73001). Both samples are currently being studied by the NASA Apollo Next Generation Sample Analysis (ANGSA) Team. The core did not reach the basal contact of the landslide deposit with the valley subfloor; therefore, a study of the slip zone is not possible. Indirect estimations of the deposit thickness have been provided by Howard et al. (1973; 10 m on average), Schmitt et al. (2017; less than 16 m near the base of the slope and about 3 m in the distal area), and Magnarini et al. (2021; up to tens of meters in the most proximal areas of the deposit). These estimations suggest that the core material is only a small fraction of the deposit and that it may not be representative of the whole landslide. Commonly, large terrestrial long runout landslides show internal structures that suggest high, localised strain at the basal contact, and deformation of the bulk deposit with preservation of the initial stratigraphy (e.g., Dufresne et al., 2016; Genevois & Ghirotti, 2005; Selli et al., 1964; Weidinger et al., 2014). However, the Light Mantle landslide's mode of emplacement remains undetermined, therefore, a turbulent granular flow mode cannot be excluded. If turbulence was involved in the emplacement of the Light Mantle landslide, clasts that have experienced strong basal deformation may have been brought to the upper part of the deposit and may be able to be identified in the Apollo 17 core sample.

Initial observations of the clast fabric and morphology in the Apollo 17 core sample show that some clasts in sample 73002 are characterised by a corona (at times discontinuous, at times continuous) of finer clast fragments (Magnarini et al., 2023), which resembles the Clast-Cortex Aggregates (CCAs) described in this work. Even though the core sample may no longer yield pristine deposit structures because of the relentless action of space weathering and micrometeoric

impacts, recognition of the microstructures of the clasts within the core sample will be a critical step towards interpreting the mechanical behaviour of the Light Mantle landslide.

5 Conclusions

We performed laboratory friction experiments using anorthosite-bearing gouges to investigate the origin of the hypermobility of the lunar Light Mantle landslide by assessing the occurrence of friction weakening mechanisms, which are responsible for the early stage instability that leads to catastrophic failure on Earth. The anorthositic material appears to have high dynamic shear strength. No evidence of dynamic weakening is seen at conditions for which it occurs in other materials. This result suggests that friction weakening mechanisms did not take place during the initiation of the Light Mantle landslide, therefore other mechanisms must have dominated the landslide emplacement and be responsible for its excessive runout distance. It is possible that the observed microstructures, such as clast-cortex aggregates, formed during the emplacement of the Light Mantle landslide. Therefore, our experimental work could be used as reference during the analysis of the microstructures and grain fabric of the core samples extracted from the landslide deposit by the Apollo 17 astronauts.

Open Research

The frictional experiments, XRD analysis, and the observational data used in this work are published as Magnarini et al. (2022).

References

Alonso, E. E., & Pinyol, N. M. (2010). Criteria for rapid sliding I. A review of Vaiont case. *Engineering Geology*, *114*(3), 198–210. https://doi.org/10.1016/j.enggeo.2010.04.018

Anders, M. H., Fouke, B. W., Zerkle, A. L., Tavarnelli, E., Alvarez, W., & Harlow, G. E. (2010). The Role of Calcining and Basal Fluidization in the Long Runout of Carbonate Slides: An Example from the Heart Mountain Slide Block, Wyoming and Montana, U.S.A. *The Journal of Geology*, *118*(6), 577–599. https://doi.org/10.1086/656383

Aretusini, S., Núñez-Cascajero, A., Spagnuolo, E., Tapetado, A., Vázquez, C., & Di Toro, G. (2021). Fast and Localized Temperature Measurements During Simulated Earthquakes in Carbonate Rocks. *Geophysical Research Letters, 48(9)*, e2020GL091856. https://doi.org/10.1029/2020GL091856

Beddingfield, C. B., Beyer, R. A., Singer, K. N., McKinnon, W. B., Runyon, K., Grundy, W., et al. (2020). Landslides on Charon. *Icarus*, *335*, 113383. https://doi.org/10.1016/j.icarus.2019.07.017

Bell, S. K., Joy, K. H., Nottingham, M., Tartese, R., Jones, R. H., Kent, J. J., et al. (2022). Initial petrographic analysis of Apollo 17 73002 continuous core thin sections using QEMSCAN mapping techniques. *53rd Lunar and Planetary Science Conference*, Abstract (1947).

Beutner, E. C., & Gerbi, G. P. (2005). Catastrophic emplacement of the Heart Mountain block slide, Wyoming and Montana, USA. *GSA Bulletin*, *117*(5–6), 724–735. https://doi.org/10.1130/B25451.1

Bickel, V. T., Aaron, J., Manconi, A., & Loew, S. (2021). Global Drivers and Transport Mechanisms of Lunar Rockfalls. *Journal of Geophysical Research: Planets*, *126*(10), e2021JE006824. https://doi.org/10.1029/2021JE006824

Bickel, V. T., Loew, S., Aaron, J., & Goedhart, N. (2022). A Global Perspective on Lunar Granular Flows. *Geophysical Research Letters*, *49*(12), e2022GL098812. https://doi.org/10.1029/2022GL098812

Boutareaud, S., Boullier, A.-M., Andréani, M., Calugaru, D.-G., Beck, P., Song, S.-R., & Shimamoto, T. (2010). Clay clast aggregates in gouges: New textural evidence for seismic

faulting. *Journal of Geophysical Research: Solid Earth*, *115*(B2). https://doi.org/10.1029/2008JB006254

Bromwell, L. G. (1966). The friction of quartz in high vacuum. *Massachusetts Institute of Technology, Cambridge, Soil Mechanics Division.*

Carrier, W. D., Bromwell, L. G., & Martin, T. R. (1972). Strength and compressibility of returned lunar soil. *Proceedings of the Lunar Science Conference,* Vol. 3, 3223-3234, The M.I.T. Press.

Carrier, W. D., Olhoeft, G. R., & Mendell, W. (1991). Physical Properties of the Lunar Surface. *In Lunar Sourcebook* (pp. 475–594). Cambridge University Press.

Cornelio, C., Spagnuolo, E., Di Toro, G., Nielsen, S., & Violay, M. (2019). Mechanical behaviour of fluid-lubricated faults. *Nature Communications, 10(1)*, 1274. https://doi.org/10.1038/s41467-019-09293-9

Di Toro, G., Hirose, T., Nielsen, S., Pennacchioni, G., & Shimamoto, T. (2006). Natural and Experimental Evidence of Melt Lubrication of Faults During Earthquakes. *Science, 311(5761)*, 647–649. https://doi.org/10.1126/science.1121012

Di Toro, G., Goldsby, D. L., & Tullis, T. E. (2004). Friction falls towards zero in quartz rock as slip velocity approaches seismic rates. Nature, 427(6973), 436–439. https://doi.org/10.1038/nature02249

Di Toro, G., Niemeijer, A., Tripoli, A., Nielsen, S., Di Felice, F., Scarlato, P., et al. (2010). From field geology to earthquake simulation: a new state-of-the-art tool to investigate rock friction during the seismic cycle (SHIVA). *RENDICONTI LINCEI*, *21*(1), 95–114. https://doi.org/10.1007/s12210-010-0097-x

Dufresne, A., Bösmeier, A., & Prager, C. (2016). Sedimentology of rock avalanche deposits – Case study and review. *Earth-Science Reviews*, *163*, 234–259. https://doi.org/10.1016/j.earscirev.2016.10.002

Erismann. (1979). Mechanisms of large landslides. *Rock Mechanics*, *12*(1), 15–46. https://doi.org/10.1007/BF01241087

Erismann, Th., Heuberger, H., & Preuss, E. (1977). The fused rock of Köfels (Tyrol) - a "Frictionite" generated by a landslide. *TMPM Tschermaks Mineralogische und Petrographische Mitteilungen*, *24*(1–2), 67–119. https://doi.org/10.1007/BF01081746

Ferri, F., Di Toro, G., Hirose, T., Han, R., Noda, H., Shimamoto, T., et al. (2011). Low- to high-velocity frictional properties of the clay-rich gouges from the slipping zone of the 1963 Vaiont slide, northern Italy. *Journal of Geophysical Research: Solid Earth*, *116*(B9). https://doi.org/10.1029/2011JB008338

Fondriest, M., Smith, S. A. F., Candela, T., Nielsen, S. B., Mair, K., & Di Toro, G. (2013). Mirror-like faults and power dissipation during earthquakes. *Geology, 41(11)*, 1175–1178. https://doi.org/10.1130/G34641.1

Genevois, R., & Ghirotti, M. (2005). The 1963 vaiont landslide. *Giornale Di Geologia Applicata*, *1*(1), 41–52.

Goren, L., & Aharonov, E. (2007). Long runout landslides: The role of frictional heating and hydraulic diffusivity. *Geophysical Research Letters*, *34*(7). https://doi.org/10.1029/2006GL028895

Goren, L., Aharonov, E., & Anders, M. H. (2010). The long runout of the Heart Mountain landslide: Heating, pressurization, and carbonate decomposition. *Journal of Geophysical Research: Solid Earth*, *115*(B10). https://doi.org/10.1029/2009JB007113

Hahn, T. M., Watkins, R. N., Robinson, M. S., Jolliff, B. L., & Louis, S. (2019). Assessing formation mechanisms for the South Massif Light Mantle deposit. *Lunar and Planetary Science Conference*, Abstract (2132).

Howard, K. A. (1973). Avalanche Mode of Motion: Implications from Lunar Examples. *Science*, *180*(4090), 1052–1055. https://doi.org/10.1126/science.180.4090.1052

Hsü, K. J. (1975). Catastrophic Debris Streams (Sturzstroms) Generated by Rockfalls. *Geological Society of America Bulletin*, *86*(1), 129. https://doi.org/10.1130/0016-7606(1975)86<129:CDSSGB>2.0.CO;2

Hu, W., Huang, R., McSaveney, M., Zhang, X., Yao, L., & Shimamoto, T. (2018). Mineral changes quantify frictional heating during a large low-friction landslide. *Geology*, *46*(3), 223–226. https://doi.org/10.1130/G39662.1

Hughes, A., Kendrick, J. E., Salas, G., Wallace, P. A., Legros, F., Di Toro, G., & Lavallée, Y. (2020). Shear localisation, strain partitioning and frictional melting in a debris avalanche generated by volcanic flank collapse. *Journal of Structural Geology*, *140*, 104132. https://doi.org/10.1016/j.jsg.2020.104132

Hurwitz, D., & Kring, D. A. (2016). Identifying the geologic context of Apollo 17 impact melt breccias. *Earth and Planetary Science Letters*, *436*, 64–70. https://doi.org/10.1016/j.epsl.2015.12.032

Ibañez, J. P., & Hatzor, Y. H. (2018). Rapid sliding and friction degradation: Lessons from the catastrophic Vajont landslide. *Engineering Geology*, *244*, 96–106. https://doi.org/10.1016/j.enggeo.2018.07.029

Kokelaar, B. P., Bahia, R. S., Joy, K. H., Viroulet, S., & Gray, J. M. N. T. (2017). Granular avalanches on the Moon: Mass-wasting conditions, processes, and features. *Journal of Geophysical Research: Planets*, *122*(9), 1893–1925. https://doi.org/10.1002/2017JE005320

Iverson, R. M. (1997). The physics of debris flows. *Reviews of Geophysics*, *35*(3), 245–296. https://doi.org/10.1029/97RG00426

Legros, F., Cantagrel, J., & Devouard, B. (2000). Pseudotachylyte (Frictionite) at the Base of the Arequipa Volcanic Landslide Deposit (Peru): Implications for Emplacement Mechanisms. *The Journal of Geology*, *108*(5), 601–611. https://doi.org/10.1086/314421

Legros, F. (2002). The mobility of long-runout landslides. *Engineering Geology*, *63*(3), 301–331. https://doi.org/10.1016/S0013-7952(01)00090-4

Lucas, A., Mangeney, A., & Ampuero, J. P. (2014). Frictional velocity-weakening in landslides on Earth and on other planetary bodies. *Nature Communications*, *5*(1), 3417. https://doi.org/10.1038/ncomms4417

Lucchitta, B. K. (1977). Crater clusters and light mantle at the Apollo 17 site; A result of secondary impact from Tycho. *Icarus*, *30*(1), 80–96. https://doi.org/10.1016/0019-1035(77)90123-3

Magnarini, G., Mitchell, T. M., Grindrod, P. M., Schmitt, H. H., & Petro, N. E. (2021). Scaling Relationship Between the Wavelength of Longitudinal Ridges and the Thickness of Long Runout Landslides on the Moon. *Journal of Geophysical Research: Planets*, *126*(10), e2021JE006922. https://doi.org/10.1029/2021JE006922

Magnarini, G., Aretusini, S., Mitchell, T. M., Pennacchioni, G., Di Toro, G., & Schmitt, H. H. (2022). Lunar analogue friction experiments [Dataset]. *Figshare*. https://doi.org/10.6084/m9.figshare.20432052.v2

Magnarini, G., Bell, S. K., Mitchell, T. M., Grindrod, P. M., Eckley, S., Joy, K. H., et al. (2023). Investigation of the Light Mantle landslide deposit emplacement dynamics through clast fabric and morphology in the Apollo 17 core sample 73002. *11th European Lunar Symposium*, June 27-29, Padua, Italy.

Melosh, H. J. (1979). Acoustic fluidization: A new geologic process? *Journal of Geophysical Research: Solid Earth*, *84*(B13), 7513–7520. https://doi.org/10.1029/JB084iB13p07513

Mitchell, T. M., Smith, S. A. F., Anders, M. H., Di Toro, G., Nielsen, S., Cavallo, A., & Beard, A. D. (2015). Catastrophic emplacement of giant landslides aided by thermal decomposition: Heart Mountain, Wyoming. *Earth and Planetary Science Letters*, *411*, 199–207. https://doi.org/10.1016/j.epsl.2014.10.051

Mizoguchi, K., Hirose, T., Shimamoto, T., & Fukuyama, E. (2007). Reconstruction of seismic faulting by high-velocity friction experiments: An example of the 1995 Kobe earthquake. *Geophysical Research Letters, 34(1)*. https://doi.org/10.1029/2006GL027931

Morrow, C. A., Moore, D. E., & Lockner, D. A. (2000). The effect of mineral bond strength and adsorbed water on fault gouge frictional strength. *Geophysical Research Letters, 27(6)*, 815–818. https://doi.org/10.1029/1999GL008401.

Niemeijer, A., Di Toro, G., Nielsen, S., & Di Felice, F. (2011). Frictional melting of gabbro under extreme experimental conditions of normal stress, acceleration, and sliding velocity. *Journal of Geophysical Research: Solid Earth*, *116*(B7). https://doi.org/10.1029/2010JB008181

Passelègue, F., Spagnuolo, E., Violay, M., Nielsen, S., Di Toro, G., & Schubnel, A. (2016). Frictional evolution, acoustic emissions activity, and off-fault damage in simulated faults sheared at seismic slip rates. *Journal of Geophysical Research: Solid Earth, 121(10)*, 7490–7513. https://doi.org/10.1002/2016JB012988

Pinyol, N. M., & Alonso, E. E. (2010). Criteria for rapid sliding II.: Thermo-hydro-mechanical and scale effects in Vaiont case. *Engineering Geology*, *114*(3), 211–227. https://doi.org/10.1016/j.enggeo.2010.04.017

Rempe, M., Smith, S. A. F., Ferri, F., Mitchell, T. M., & Di Toro, G. (2014). Clast-cortex aggregates in experimental and natural calcite-bearing fault zones. *Journal of Structural Geology*, *68*, 142–157. https://doi.org/10.1016/j.jsg.2014.09.007

Rice, J. R. (2006). Heating and weakening of faults during earthquake slip. *Journal of Geophysical Research: Solid Earth*, *111*(B5). https://doi.org/10.1029/2005JB004006

Schmidt, B. E., Hughson, K. H. G., Chilton, H. T., Scully, J. E. C., Platz, T., Nathues, A., et al. (2017). Geomorphological evidence for ground ice on dwarf planet Ceres. *Nature Geoscience*, *10*(5), 338–343. https://doi.org/10.1038/ngeo2936

Schmitt, H. H., & Cernan, E. A. (1973, January 1). A geological investigation of the Taurus-Littrow Valley. Retrieved from https://ntrs.nasa.gov/citations/19740010322

Schmitt, H. H., Petro, N. E., Wells, R. A., Robinson, M. S., Weiss, B. P., & Mercer, C. M. (2017). Revisiting the field geology of Taurus–Littrow. *Icarus*, *298*, 2–33. https://doi.org/10.1016/j.icarus.2016.11.042

Selli, R., Trevisan, L., Carloni, G. C., Mazzanti, R., & Ciabatti, M. (1964). La frana del Vajont. *Giornale di Geologia*, *32*(1), 1–154.

Shearer, C. K., McCubbin, F. M., Zeigler, R. A., Gross, J., & ANGSA Science Team. (2020). Apollo Next Generation Sample Analysis (ANGSA) Initiative. Fulfilling Apollo science goals and preparing for returning to the Moon. Abstract V013-0001. *AGU Fall Meeting*, 1-20 December 2020, virtual.

Shearer, C. K., McCubbin, F. M., Zeigler, R. A., Gross, J., Simon, S. B., Meshik, A., et al. (2022). Preparing for Artemis through lessons learned from Apollo 17. Highlighting the progress of the ANGSA initiative. *53rd Lunar and Planetary Science Conference*, Abstract (2546).

Shimamoto, T., & Logan, J. M. (1981). Effects of simulated clay gouges on the sliding behavior of Tennessee sandston. *Tectonophysics, 75(3)*, 243–255. https://doi.org/10.1016/0040-1951(81)90276-6.

Simon, S. B., Cato, M. J., Shearer, C. K., & ANGSA Science Team. (2022). Results from the 1mm to 150μm fraction of Apollo 17 drive tube 73002: modal petrology and new rock types (Vol. 2211). *53rd Lunar and Planetary Science Conference*, Abstract (2211).

Singer, K. N., McKinnon, W. B., Schenk, P. M., & Moore, J. M. (2012). Massive ice avalanches on Iapetus mobilized by friction reduction during flash heating. *Nature Geoscience*, *5*(8), 574–578. https://doi.org/10.1038/ngeo1526

Smith, S. A. F., Billi, A., Toro, G. D., & Spiess, R. (2011). Principal Slip Zones in Limestone: Microstructural Characterization and Implications for the Seismic Cycle (Tre Monti Fault, Central Apennines, Italy). *Pure and Applied Geophysics*, *168*(12), 2365–2393. https://doi.org/10.1007/s00024-011-0267-5

Smith, S. A. F., Nielsen, S., & Di Toro, G. (2015). Strain localization and the onset of dynamic weakening in calcite fault gouge. *Earth and Planetary Science Letters, 413*, 25–36. https://doi.org/10.1016/j.epsl.2014.12.043

Sun, L., Taylor, G. J., Martel, L. M. V., & Lucey, P. (2022). A comprehensive study of mineralogy at Apollo 17 landing site. *53rd Lunar and Planetary Science Conference*, Abstract (1693).

Vardoulakis. (2000). Catastrophic landslides due to frictional heating of the failure plane. *Mechanics of Cohesive-Frictional Materials*, *5*(6), 443–467. https://doi.org/10.1002/1099-1484(200008)5:6<443::AID-CFM104>3.0.CO;2-W

Vardoulakis. (2002). Dynamic thermo-poro-mechanical analysis of catastrophic landslides. *Géotechnique*, *52*(3), 157–171. https://doi.org/10.1680/geot.2002.52.3.157

Veveakis, E., Vardoulakis, I., & Di Toro, G. (2007). Thermoporomechanics of creeping landslides: The 1963 Vaiont slide, northern Italy. *Journal of Geophysical Research: Earth Surface*, *112*(F3). https://doi.org/10.1029/2006JF000702

Viesca, R. C., & Rice, J. R. (2012). Nucleation of slip-weakening rupture instability in landslides by localized increase of pore pressure. *Journal of Geophysical Research: Solid Earth*, *117*(B3). https://doi.org/10.1029/2011JB008866

Violay, M., Nielsen, S., Gibert, B., Spagnuolo, E., Cavallo, A., Azais, P., et al. (2014). Effect of water on the frictional behavior of cohesive rocks during earthquakes. *Geology, 42(1)*, 27–30. https://doi.org/10.1130/G34916.1

Violay, M., Di Toro, G., Nielsen, S., Spagnuolo, E., & Burg, J. P. (2015). Thermo-mechanical pressurization of experimental faults in cohesive rocks during seismic slip. *Earth and Planetary Science Letters, 429*, 1–10. https://doi.org/10.1016/j.epsl.2015.07.054

Voight, B., & Faust, C. (1982). Frictional heat and strength loss in some rapid landslides. *Géotechnique*, *32*(1), 43–54. https://doi.org/10.1680/geot.1982.32.1.43

Wang, Y. F., Dong, J. J., & Cheng, Q. G. (2017). Velocity-dependent frictional weakening of large rock avalanche basal facies: Implications for rock avalanche hypermobility? *Journal of Geophysical Research: Solid Earth*, *122*(3), 1648–1676. https://doi.org/10.1002/2016JB013624

Watkins, J. A., Ehlmann, B. L., & Yin, A. (2015). Long-runout landslides and the long-lasting effects of early water activity on Mars. *Geology*, *43*(2), 107–110. https://doi.org/10.1130/G36215.1

Weidinger, J. T., & Korup, O. (2009). Frictionite as evidence for a large Late Quaternary rockslide near Kanchenjunga, Sikkim Himalayas, India — Implications for extreme events in mountain relief destruction. *Geomorphology*, *103*(1), 57–65. https://doi.org/10.1016/j.geomorph.2007.10.021

Weidinger, J. T., Korup, O., Munack, H., Altenberger, U., Dunning, S. A., Tippelt, G., & Lottermoser, W. (2014). Giant rockslides from the inside. *Earth and Planetary Science Letters*, *389*, 62–73. https://doi.org/10.1016/j.epsl.2013.12.017

Ryder, G., Spudis, P. D., & Schmitt, H. H. (1992). Workshop on Geology of the Apollo 17 Landing Site. Houston, Texas December 2-4, 1992. Lunar and Planetary Institute.

Wolfe, E. W., Bailey, N. G., Lucchitta, B. K., Muehlberger, W. R., Scott, D. H., Sutton, R. L., et al. (1981). The geologic investigation of the Taurus-Littrow Valley; Apollo 17 landing site, with a section on Apollo 17 lunar surface photography (USGS Professional Paper No. 1080). https://doi.org/10.3133/pp1080

Niemeijer, A., Di Toro, G., Griffith, W. A., Bistacchi, A., Smith, S. A. F., & Nielsen, S. (2012). Inferring earthquake physics and chemistry using an integrated field and laboratory approach. Journal of Structural Geology, 39, 2–36. https://doi.org/10.1016/j.jsg.2012.02.018

Mangeney, A., Roche, O., Hungr, O., Mangold, N., Faccanoni, G., & Lucas, A. (2010). Erosion and mobility in granular collapse over sloping beds. Journal of Geophysical Research: Earth Surface, 115(F3). https://doi.org/10.1029/2009JF00146

Hörz, F., Grieve, R., Heiken, G., Spudis, P., & Binder, A. (1991). Lunar Surface Processes. In Lunar Sourcebook (pp. 61–120). Cambridge University Press.

Davies, T. R. H., & McSaveney, M. J. (2009). The role of rock fragmentation in the motion of large landslides. Engineering Geology, 109(1), 67–79. https://doi.org/10.1016/j.enggeo.2008.11.004

Davies, T. R. H. (1982). Spreading of rock avalanche debris by mechanical fluidization. Rock Mechanics, 15(1), 9–24. https://doi.org/10.1007/BF01239474

Heim, A. (1932). Der Bergsturz und Menschenleben. Zurich: Fretz und Wasmuth Verlag.

Davies, T. R. H., & McSaveney, M. J. (2012). Mobility of long-runout rock avalanches. In D. Stead & J. J. Clague (Eds.), Landslides: Types, Mechanisms and Modeling (pp. 50–58). Cambridge: Cambridge University Press. https://doi.org/10.1017/CBO9780511740367.006

Davies, T. R. H., & McSaveney, M. J. (2002). Dynamic simulation of the motion of fragmenting rock avalanches. Canadian Geotechnical Journal, 39(4), 789–798. https://doi.org/10.1139/t02-035